ALCHEMY : JOURNAL OF CHEMISTRY

Research Article

Structural, Optical, and Photocatalytic Properties of Sol-Gel-Derived ZnO Nanoparticles for Methylene Blue Degradation

Maria Luruk Seran[1], Matius Stefanus Batu[1], Cindy Claudia Christanti[1], Didi Prasetyo Benu[1]*

[1] Department of Chemistry, Universitas Timor, Kefamenanu 85613, Indonesia.

Article Info

Article History
Received 28 January 2026
Revised 03 March 2026
Accepted 04 March 2026
Available online 23 May 2026

* Email (Author Corresponding):
didibenu@unimor.ac.id

ABSTRACT

Zinc oxide (ZnO) nanoparticles are attractive photocatalysts due to their wide band gap, chemical stability, and nanoscale-dependent properties. Herein, ZnO nanoparticles were synthesized and systematically characterized to correlate their structural and optical properties with photocatalytic performance. Raman spectroscopy and *X*-ray diffraction confirmed the formation of a single-phase wurtzite ZnO structure with high crystallinity. UV-Vis diffuse reflectance spectroscopy revealed a distinct absorption edge in the UV region, and the optical band gap was determined to be 3.07 eV using the Kubelka–Munk–Tauc method. The photocatalytic activity of the synthesized ZnO was evaluated via methylene blue degradation under UV irradiation. Time-resolved UV-Vis absorption measurements showed a gradual decrease in the characteristic absorption peak at 660-670 nm, indicating effective dye degradation. A photocatalytic degradation efficiency of 60.55% was achieved after 150 min of irradiation. Kinetic analysis demonstrated that the degradation process followed pseudo-first-order kinetics with an apparent rate constant of 0.0062 min^{-1}. These results demonstrate that the synthesized ZnO nanoparticles exhibit efficient UV-driven photocatalytic activity, highlighting their potential for nanoscale photocatalyst applications. The structure–property–performance correlation established in this work provides insight for further nanostructure and defect engineering strategies to enhance photocatalytic efficiency.

Keywords: Methylene blue; photodegradation; sol-gel; structural and optical properties; ZnO photocatalyst

1. Introduction

The increasing discharge of organic dye pollutants from textile, paper, and pharmaceutical industries has raised serious environmental and public health concerns due to their toxicity, chemical stability, and resistance to conventional wastewater treatment methods [1], [2]. Among these pollutants, methylene blue is frequently used as a model organic dye because of its widespread industrial application and high persistence in aquatic environments [3], [4]. Therefore, the development of efficient and sustainable treatment technologies for dye-contaminated wastewater remains an important research focus.

Semiconductor-based photocatalysis has emerged as a promising advanced oxidation process for environmental remediation, as it enables the mineralization of organic pollutants into less harmful products under light irradiation [5], [6]. Zinc oxide (ZnO) is one of the most widely studied photocatalytic materials owing to its wide band gap, high electron mobility, non-toxicity, and good chemical stability. In addition, ZnO exhibits strong absorption in the ultraviolet region and can generate reactive oxygen species that drive photocatalytic degradation reactions [5], [6], [7]. However, the photocatalytic performance of ZnO is strongly dependent on its crystal structure, optical properties, and synthesis conditions [8], [9].

Various synthesis approaches have been employed to tailor the structural and optical characteristics of ZnO, including hydrothermal and solvothermal [5], [10], chemical vapor deposition [11], microemulsion/macroemulsion [5], [6], electrodeposition [12], and sol–gel methods [13], [14]. Hydrothermal and solvothermal techniques enable the growth of highly crystalline ZnO nanorods and hierarchical structures under controlled temperature and pressure conditions, although they require sealed reactors and longer processing times [15]. Chemical vapor deposition (CVD) produces high-quality and oriented ZnO thin films with excellent optoelectronic properties but involves high temperatures and sophisticated equipment [16]. The microemulsion method allows precise particle size control through nanoscale micellar confinement, yet it commonly relies on surfactants and organic solvents [17]. Electrodeposition offers direct growth of ZnO films on conductive substrates with tunable thickness and morphology; however, it is mainly suitable for thin-film fabrication [18]. Compared with these approaches, the sol–gel method provides a simple, low-temperature, and scalable route, enabling good compositional homogeneity and controlled nanoparticle formation in aqueous systems. Despite extensive studies, establishing a clear correlation between synthesis method, structure, optical properties, and photocatalytic activity of ZnO remains an ongoing challenge, particularly in relation to dye degradation efficiency and reaction kinetics.

In this study, ZnO nanoparticles were synthesized via the sol–gel method and systematically characterized to investigate their structural and optical properties. The photocatalytic performance of the synthesized ZnO was evaluated through the degradation of methylene blue under UV irradiation, and the reaction kinetics were analyzed using a pseudo-first-order model. By correlating structural features, band gap energy, and photocatalytic behaviour, this work aims to provide insight into the structure–property–performance relationship of ZnO photocatalysts and to support their potential application in photocatalytic wastewater treatment.

2. Materials and Methods

2.1. Materials

Zinc acetate dihydrate ($Zn(CH_3COO)_2$) and sodium hydroxide (NaOH) was purchased from Merck. All chemicals were directly used without any further purification.

2.2. Methods

2.3.1 Synthesis of ZnO

The synthesized method was adopted from Lee et al. with some modifications [19]. Zinc oxide (ZnO) nanoparticles were synthesized using the sol–gel method, with zinc acetate dihydrate ($Zn(CH_3COO)_2 \cdot 2H_2O$) serving as the precursor. A total of 2.64 g of $Zn(CH_3COO)_2 \cdot 2H_2O$ was weighed, placed into a glass bottle, and dissolved in 150 mL of deionized water under continuous stirring using a hot plate stirrer at room temperature. Subsequently, 30 mL of 0.1 M NaOH solution was added dropwise until a turbid mixture was formed. The bottle was then tightly sealed, placed in an oil bath, and the reaction was carried out at 100 °C for 2 h. After completion

of the reaction, the product suspension was allowed to cool to room temperature. The synthesized solid was separated from the solution by centrifugation. The collected precipitate was dried in an oven at 100 °C for 4 h, followed by calcination at 400 °C for 2 h.

2.3.2 Characterization

The structural properties of the synthesized particles were characterized using Raman spectroscopy and *X*-ray diffraction (XRD). The optical properties were analyzed by ultraviolet–visible diffuse reflectance spectroscopy (UV–Vis DRS). The obtained spectra were subsequently processed using the Tauc plot method based on the Kubelka–Munk function to determine the optical band gap energy.

2.3.3 Photocatalytic activity evaluation

The photocatalytic activity was evaluated using methylene blue (MB) solution as a model organic dye pollutant. A total of 50 mg of ZnO nanoparticles was dispersed in 50 mL of methylene blue solution (5 ppm) and shaken for 5 min to ensure homogeneous dispersion. Subsequently, the suspension was magnetically stirred in the dark for 5 min to establish adsorption–desorption equilibrium. The mixture was then irradiated under 395 UV-LED light for 150 min. At 30 min intervals, 5 mL aliquots were withdrawn and the photocatalyst particles were separated by centrifugation. The concentration of methylene blue in the supernatant was analyzed using UV–Vis spectroscopy.

The photocatalytic degradation kinetics were evaluated using the pseudo-first-order reaction model, as expressed by the following equation:

$$\ln\left(\frac{C_t}{C_0}\right) = -kt \qquad (1)$$

with C_t represents the concentration of methylene blue at reaction time t, C_0 is the initial concentration of methylene blue (5 ppm), t is the irradiation time, and k is the apparent first-order rate constant. The value of k was obtained from the slope of the linear plot of $\ln(C_t/C_0)$ versus irradiation time (t). In addition, the photocatalytic degradation efficiency was calculated using the following equation:

$$\eta(t) = \frac{C_0 - C_t}{C_0} \times 100\% \qquad (2)$$

with $\eta(t)$ denotes the photocatalytic degradation efficiency at time t.

3. Result and Discussion

3.1. Characteristics of The Synthesized Sample

The local structural characteristics of the synthesized ZnO particles were investigated using Raman spectroscopy. **Figure 1a** presents the Raman spectrum of the as-synthesized sample. As shown in Figure 1a, the Raman spectrum exhibits several characteristic peaks associated with ZnO. In the hexagonal wurtzite structure of ZnO (space group $P6_3mc$), the optical phonon modes at the Γ point are classified according to group theory as: $\Gamma = A_1 + 2E_2 + E_1 + 2B_1$. A_1 and E_1 modes are polar and split into transverse optical (*TO*) and longitudinal optical (*LO*) components due to long-range Coulomb interactions, E_2 modes are nonpolar and Raman active, and B_1 modes are silent (inactive in both Raman and IR spectroscopy) [20], [21], [22].

Two high-intensity peaks located at Raman shifts of approximately 100 and 439 cm^{-1} can be assigned to the E_{2L} and E_{2H} vibrational modes, respectively. In addition, the peak observed around 330 cm^{-1} corresponds to the E_{2H}–E_{2L} combination mode. The E_{2H} mode is mainly associated with oxygen atom vibrations, whereas the E_{2L} mode originates from the vibration of zinc atoms within the ZnO crystal lattice [23]. The E_{2L} mode correspond to in-plane vibrational motion (perpendicular to the *c*-axis) and reflects lattice dynamics dominated by the metal atom. Because it involves low-frequency lattice vibrations, it is sensitive to mass-related effects and long-range crystal ordering. The E_{2H} mode correspond to in-plane optical phonon vibrations of oxygen atoms and is widely

regarded as a fingerprint of highly crystalline wurtzite ZnO [20], [21], [22]. These Raman features clearly indicate that the synthesized particles possess a wurtzite ZnO crystal structure.

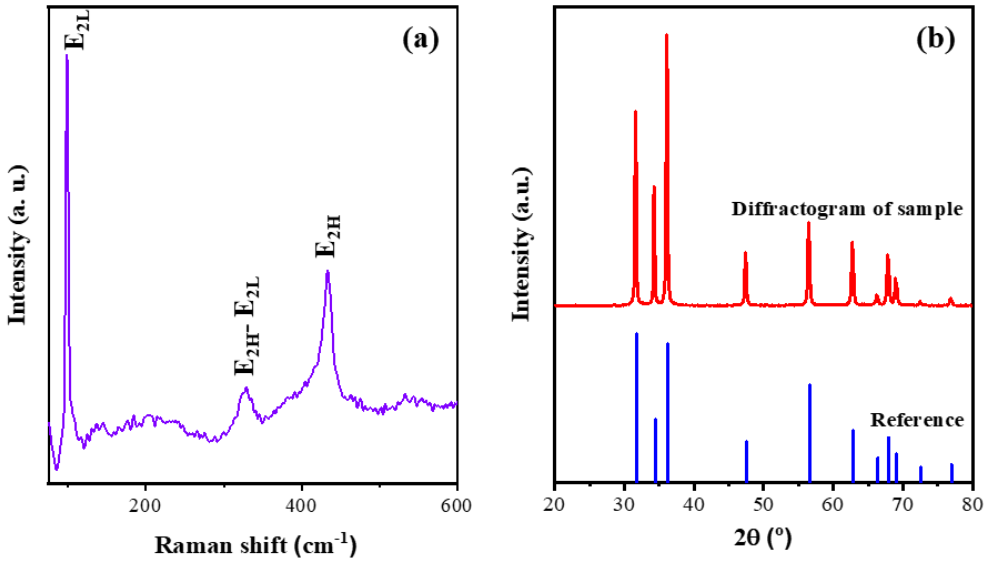

Figure 1. Structural characterization of the synthesized sample; (a) Raman spectra, (b) XRD pattern along with the corresponding CIF reference file No. 2300450.

To further confirm the global crystal structure and phase purity, the synthesized sample was also characterized by X-ray diffraction (XRD). The XRD pattern of the sample, along with the corresponding CIF reference file No. 2300450, is shown in **Figure 1b**. The reference CIF file of wurtzite ZnO was obtained from crystallography open database (COD) website. The diffraction peaks exhibit excellent agreement with the reference data, confirming that the synthesized material is ZnO with a wurtzite crystal structure and a $P6_3mc$ space group [24]. This structural assignment is supported by the presence of three dominant diffraction peaks at 2θ values of approximately 31.59°, 34.26°, and 36.08°, which correspond to the (100), (002), and (101) crystallographic planes, respectively [24]. Additional diffraction peaks with lower intensities are also observed and closely match those of the reference pattern. Notably, no impurity-related peaks are detected, indicating that the synthesized ZnO exhibits high phase purity. We also calculate the crystallite size of samples from the three main peaks using Scherrer equation. The results show that the crystallite size at direction of [100], [002], and [101] is 69.51, 70.56, and 65.10 nm, respectively. The crystallite size indicates that the synthesized sample is a nanocrystal.

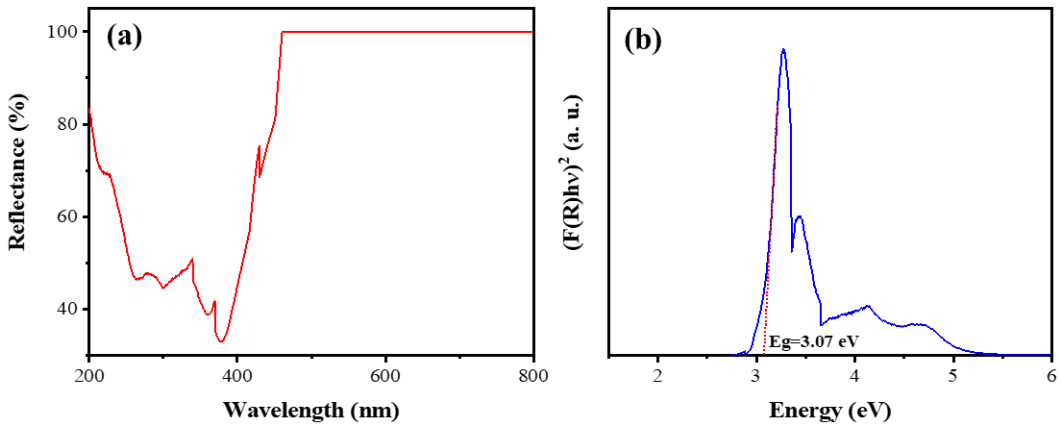

Figure 2. (a) UV-Vis DRS spectra of synthesized particles; (b) Tauc plot for direct bandgap to determine the bandgap energy.

The optical properties of the ZnO particles were investigated using UV–Vis diffuse reflectance spectroscopy (UV–Vis DRS). The UV–Vis DRS spectrum of the as-synthesized ZnO sample is shown in **Figure 2a**. The spectra exhibit a sharp decrease in reflectance is observed in the wavelength range of approximately 350-450 nm, which corresponds to the characteristic absorption edge of ZnO as a wide-band-gap semiconductor.

The strong light absorption in this region is attributed to electronic transitions from the valence band to the conduction band [25]. The optical band gap energy (E_g) of the synthesized ZnO particles was determined using the Tauc plot method based on the Kubelka–Munk approach, as shown in **Figure 2b**. The analysis indicates that the as-synthesized ZnO exhibits a band gap energy of 3.07 eV.

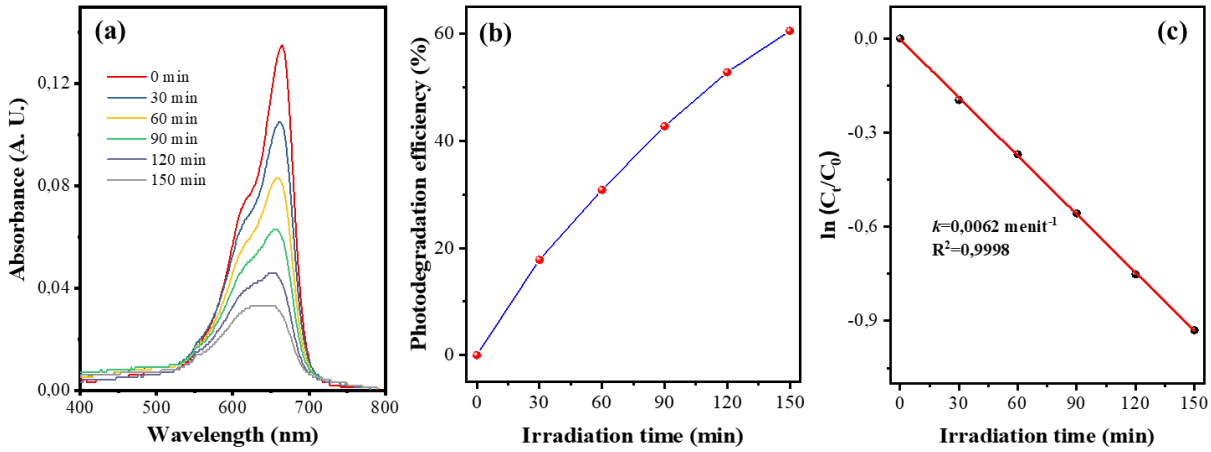

Figure 3. Photocatalytic evaluation of the synthesized ZnO; (a) evolution of MB absorption spectra, (b) photodegradation efficiency, (c) pseudo-first-order kinetic plot.

3.2. Photocatalytic Activity

The photocatalytic activity of ZnO was evaluated through the degradation of methylene blue under UV irradiation. **Figure 3a** shows the temporal evolution of the UV–Vis absorption spectra of methylene blue during the photocatalytic degradation process in the presence of the as-synthesized ZnO photocatalyst. As observed in **Figure 3a**, the intensity of the characteristic absorption peak of methylene blue at around 660–670 nm gradually decreases with increasing irradiation time. This progressive decrease in absorbance indicates a continuous reduction in methylene blue concentration due to photocatalytic degradation. The obtained spectral data were further processed to calculate the photocatalytic degradation efficiency.

Figure 3b presents the variation of the photocatalytic degradation efficiency of methylene blue as a function of irradiation time. In general, the degradation efficiency increases with prolonged irradiation. At the initial stage of the reaction, the efficiency increases relatively rapidly, which can be attributed to the high availability of active sites on the photocatalyst surface and the relatively high dye concentration. At longer irradiation times, the rate of efficiency increase tends to slow down as the dye concentration decreases and the system approaches a saturation condition [3]. After 150 min of UV irradiation, a photocatalytic degradation efficiency of 60.55% was achieved.

The pseudo-first-order kinetic plot for methylene blue degradation using the synthesized ZnO photocatalyst is shown in **Figure 3c**. As depicted in **Figure 3c**, a linear relationship between $\ln(C_t/C_0)$ and irradiation time is obtained for the sample, indicating that the photocatalytic degradation process follows pseudo-first-order kinetics. The high coefficient of determination (R^2) confirms a good agreement between the experimental data and the applied kinetic model. This behavior is consistent with the characteristics of heterogeneous photocatalytic reactions at relatively low dye concentrations [26]. Furthermore, the apparent rate constant (k) obtained from the slope of the linear fit is 0.0062 min^{-1}, demonstrating that the synthesized ZnO effectively facilitates the photocatalytic degradation reaction with a relatively high reaction rate.

Here, we also compared the photocatalytic activity in this work and the data reported from recent articles. The data can be seen in **Table 1.** The data comparison shows that the synthesized ZnO has higher photocatalytic activity under UV irradiation that the data reported Elsisi et al. and by Atta et al. [27], [28]. However, it was still a challenge to enhance the photocatalytic activity especially under sunlight or visible light irradiation. The synthesized ZnO has bandgap energy about 3,07 eV, which is only has high activity under UV light irradiation. Some modifications should be performed to enhance the photocatalytic activity under visible light irradiation including metal doping, heterojunction construction, and so on.

Table 1. Photocatalytic activity of the synthesized ZnO compared with the data from several previously reported articles

Sample	Synthesized method	Light source	Catalyst loading (g/L)	Photodegradation efficiency	*k* (min $^{-1}$)	Refs.
ZnO nanocrystal	Sol-gel	395 nm UV LED	1	60.55% in 150 min	6.2×10^{-3}	This work
ZnO nanoparticle	Sol-gel	UV light	3	58.79% in 60 min	4.5×10^{-3}	[27]
ZnO thin film	Sol-gel	305 nm laser	NA	60% in 24 h	5.1×10^{-3}	[28]
ZnO nanoparticle	Sol-gel	Sunlight	2	100 % in 180 min	1.95×10^{-2}	[29]
ZnO thin film	Sol-gel	17 W cold white light	NA	NA	2.0×10^{-4}	[30]
ZnO nanoparticle	Sol-gel	Sunlight	1	77% in 120 min	1.14×10^{-2}	[31]
ZnO nanoparticle	Sol-gel	150 W mercury light	1	±80% in 180 min	1.07×10^{-2}	[32]

4. Conclusion

ZnO nanoparticles were successfully synthesized and exhibited a single-phase wurtzite crystal structure, as confirmed by Raman spectroscopy and *X*-ray diffraction. UV–Vis diffuse reflectance analysis revealed a characteristic UV absorption edge, and the optical band gap energy was determined to be 3.07 eV using the Kubelka–Munk–Tauc approach. The synthesized ZnO demonstrated effective photocatalytic activity toward methylene blue degradation under UV irradiation, achieving a degradation efficiency of 60.55% after 150 min. Kinetic analysis showed that the degradation followed pseudo-first-order behaviour with an apparent rate constant of 0.0062 min^{-1}. The established correlation between structure, optical properties, and photocatalytic performance provides a basis for further material optimization to enhance efficiency and extend activity toward visible-light-driven environmental applications.

Acknowledgement

The research was financially supported by LPPM Universitas Timor through basic research grant 2025. DPB thanks to Prof. Veinardi Suendo for the support of sample characterization using Raman spectroscopy.

References

[1] H. N. Abdelhamid, "Photocatalytic degradation of organic dyes using ZIF-67," *Surf. Interfaces*, vol. 73, p. 107580, Sep. 2025, doi: 10.1016/j.surfin.2025.107580.

[2] A. S. Belousov *et al.*, "Regulating of MnO_2 photocatalytic activity in degradation of organic dyes by polymorphic engineering," *Solid State Sci.*, vol. 132, p. 106997, Oct. 2022, doi: 10.1016/j.solidstatesciences.2022.106997.

[3] J. N. Tsaviv, I. S. Eneji, R. Sha'Ato, I. Ahemen, P. R. Jubu, and Y. Yusof, "Photodegradation, kinetics and non-linear error functions of methylene blue dye using $SrZrO_3$ perovskite photocatalyst," *Heliyon*, vol. 10, no. 14, p. e34517, Jul. 2024, doi: 10.1016/j.heliyon.2024.e34517.

[4] S. Rasheed *et al.*, "Photocatalytic Degradation of Methylene Blue by Engineering Tungstic Acid@ZIF-67 Cocatalyst," *ChemistrySelect*, vol. 9, no. 46, p. e202403807, Dec. 2024, doi: 10.1002/slct.202403807.

[5] D. P. Benu *et al.*, "Macroemulsion-mediated synthesis of fibrous ZnO microrods and their surface morphology contribution to the high photocatalytic degradation rate," *New J. Chem.*, vol. 47, no. 1, pp. 428–442, 2023, doi: 10.1039/D2NJ04862K.

[6] A. Andriani *et al.*, "Role of urea on the structural, textural, and optical properties of macroemulsion-assisted synthesized holey ZnO nanosheets for photocatalytic applications," *New J. Chem.*, vol. 46, no. 20, pp. 9897–9908, 2022, doi: 10.1039/D2NJ00184E.

[7] C. C. Christanti and D. P. Benu, "Low-Temperature Synthesis of ZnO Nanoparticles Using a Water-Methanol Solvent for Rhodamine B Photodegradation," *J. Beta Kim.*, vol. 5, no. 1, pp. 62–69, Apr. 2025, doi: 10.35508/jbk.v5i1.21305.

[8] V. Nedelkovski, M. Radovanović, and M. Antonijević, "Advances in Photocatalytic Degradation of Crystal Violet Using ZnO-Based Nanomaterials and Optimization Possibilities: A Review," *ChemEngineering*, vol. 9, no. 6, p. 120, 2025, doi: 10.3390/chemengineering9060120.

[9] T. Rodríguez-Flores, I. Hernández-Pérez, G. E. de la Huerta-Hernández, Y. Ayala-Parada, J. G. Cadena-Silva, and C. Haro-Pérez, "Comparison of Photocatalytic Performance of Sonochemically Synthesized ZnO with Different Capping Agents," *ACS Omega*, vol. 10, no. 28, pp. 30181–30193, Jul. 2025, doi: 10.1021/acsomega.5c00929.

[10] C. C. Christanti and D. P. Benu, "Sintesis ZnO Berstruktur Nano Menggunakan Campuran Pelarut Air-Etilen Glikol dan Karakterisasi Struktur, Morfologi, dan Energi Celah Pita Partikel," *J. Chem. Sci. App.*, vol. 2, no. 2, pp. 27–30, 2024.

[11] I. A. Ahmad and Y. H. Mohammed, "Synthesis of ZnO nanowires by thermal chemical vapor deposition technique: Role of oxygen flow rate," *Micro Nanostructures*, vol. 181, p. 207628, Sep. 2023, doi: 10.1016/j.micrna.2023.207628.

[12] Y.-H. Huang, Y.-T. Chuang, H.-W. Lin, and C.-N. Liao, "Single-Step Electrodeposition of ZnO Nanoparticles Decorated (111)-Textured Cu_2O Films with Enhanced Photoelectrochemical Properties," *Inorg. Chem.*, vol. 64, no. 33, pp. 16950–16959, Aug. 2025, doi: 10.1021/acs.inorgchem.5c02573.

[13] J. N. Hasnidawani, H. N. Azlina, H. Norita, N. N. Bonnia, S. Ratim, and E. S. Ali, "Synthesis of ZnO Nanostructures Using Sol-Gel Method," *5th Int. Conf. Recent Adv. Mater. Miner. Environ. RAMM 2nd Int. Postgrad. Conf. Mater. Miner. Polym. MAMIP*, vol. 19, pp. 211–216, Jan. 2016, doi: 10.1016/j.proche.2016.03.095.

[14] S. Kanwal, M. Tahir Khan, V. Tirth, A. Algahtani, T. Al-Mughanam, and A. Zaman, "Room-Temperature Ferromagnetism in Mn-Doped ZnO Nanoparticles Synthesized by the Sol–Gel Method," *ACS Omega*, vol. 8, no. 31, pp. 28749–28757, Aug. 2023, doi: 10.1021/acsomega.3c03418.

[15] J. C. Anaya-Zavaleta *et al.*, "ZnO Nanoparticles by Hydrothermal Method: Synthesis and Characterization," *Technologies*, vol. 13, no. 1, p. 18, 2025, doi: 10.3390/technologies13010018.

[16] J. Pei *et al.*, "Advancements in the Synthesis and Functionalization of Zinc Oxide-Based Nanomaterials for Enhanced Oral Cancer Therapy," *Molecules*, vol. 29, no. 11, p. 2706, 2024, doi: 10.3390/molecules29112706.

[17] Y. Wang, X. Zhang, A. Wang, X. Li, G. Wang, and L. Zhao, "Synthesis of ZnO nanoparticles from microemulsions in a flow type microreactor," *Chem. Eng. J.*, vol. 235, pp. 191–197, Jan. 2014, doi: 10.1016/j.cej.2013.09.020.

[18] M. Kumar and C. Sasikumar, "Electrodeposition of Nanostructured ZnO Thin Film: A Review," *Am. J. Mater. Sci. Eng.*, vol. 2, no. 2, pp. 18–23, May 2014, doi: 10.12691/ajmse-2-2-2.

[19] J. Lee, A. J. Easteal, U. Pal, and D. Bhattacharyya, "Evolution of ZnO nanostructures in sol–gel synthesis," *Curr. Appl. Phys.*, vol. 9, no. 4, pp. 792–796, Jul. 2009, doi: 10.1016/j.cap.2008.07.018.

[20] R. Cuscó *et al.*, "Temperature dependence of Raman scattering in ZnO," *Phys. Rev. B*, vol. 75, no. 16, p. 165202, Apr. 2007, doi: 10.1103/PhysRevB.75.165202.

[21] M. Manica *et al.*, "Morphological and Optical Properties of RE-Doped ZnO Thin Films Fabricated Using Nanostructured Microclusters Grown by Electrospinning–Calcination," *Nanomaterials*, vol. 15, no. 17, p. 1369, 2025, doi: 10.3390/nano15171369.

[22] M. Šćepanović, M. Grujić-Brojčin, K. Vojisavljević, S. Bernik, and T. Srećković, "Raman study of structural disorder in ZnO nanopowders," *J. Raman Spectrosc.*, vol. 41, no. 9, pp. 914–921, Sep. 2010, doi: 10.1002/jrs.2546.

[23] S. Marković *et al.*, "Effect of PEO molecular weight on sunlight induced photocatalytic activity of ZnO/PEO composites," *Sol. Energy*, vol. 127, pp. 124–135, Apr. 2016, doi: 10.1016/j.solener.2016.01.026.

[24] M. Schreyer, L. Guo, S. Thirunahari, F. Gao, and M. Garland, "Simultaneous determination of several crystal structures from powder mixtures: the combination of powder X-ray diffraction, band-target entropy minimization and Rietveld methods," *J. Appl. Crystallogr.*, vol. 47, no. 2, pp. 659–667, Apr. 2014, doi: 10.1107/S1600576714003379.

[25] S. Anandan, N. Ohashi, and M. Miyauchi, "ZnO-based visible-light photocatalyst: Band-gap engineering and multi-electron reduction by co-catalyst," *Appl. Catal. B Environ.*, vol. 100, no. 3, pp. 502–509, Oct. 2010, doi: 10.1016/j.apcatb.2010.08.029.

[26] Y. M. Manawi, Ihsanullah, A. Samara, T. Al-Ansari, and M. A. Atieh, "A Review of Carbon Nanomaterials' Synthesis via the Chemical Vapor Deposition (CVD) Method," *Materials*, vol. 11, no. 5, p. 822, May 2018, doi: 10.3390/ma11050822.

[27] Moustafa. E. Elsisi, M. M. Mostafa, H. Abdella, A. E. Khalil, and A. S. Soror, "In-depth investigation the size effect of zinc oxide nanostructures on the photodegradation of different dyes under UV-irradiation: anticancer application," *Sci. Rep.*, vol. 15, no. 1, p. 31669, Aug. 2025, doi: 10.1038/s41598-025-16270-4.

[28] D. Atta, H. A. Wahab, M. A. Ibrahim, and I. K. Battisha, "Photocatalytic degradation of methylene blue dye by ZnO nanoparticle thin films, using Sol–gel technique and UV laser irradiation," *Sci. Rep.*, vol. 14, no. 1, p. 26961, Nov. 2024, doi: 10.1038/s41598-024-76938-1.

[29] N. Fathy, S. Fathy, F. Ali, and S. Mousa, "Effective sunlight photodegradation of methylene blue dye using zinc oxide doped with mono- and bi-metals of Ag and Ce," *Desalination Water Treat.*, vol. 320, p. 100595, Oct. 2024, doi: 10.1016/j.dwt.2024.100595.

[30] W. Vallejo, A. Cantillo, and C. Díaz-Uribe, "Methylene Blue Photodegradation under Visible Irradiation on Ag-Doped ZnO Thin Films," *Int. J. Photoenergy*, vol. 2020, pp. 1–11, Jan. 2020, doi: 10.1155/2020/1627498.

[31] P. Eswaran, P. D. Madasamy, K. Pillay, and H. Brink, "Sunlight-driven photocatalytic degradation of methylene blue using ZnO/biochar nanocomposite derived from banana peels," *Biomass Convers. Biorefinery*, vol. 15, no. 8, pp. 12347–12367, Apr. 2025, doi: 10.1007/s13399-024-05999-z.

[32] K. A. Isai and V. S. Shrivastava, "Photocatalytic degradation of methylene blue using ZnO and 2%Fe–ZnO semiconductor nanomaterials synthesized by sol–gel method: a comparative study," *SN Appl. Sci.*, vol. 1, no. 10, p. 1247, Oct. 2019, doi: 10.1007/s42452-019-1279-5.